Genes & Diseases (2019) 6, 56–67

Available online at www.sciencedirect.com

ScienceDirect

journal homepage: http://ees.elsevier.com/gendis/default.asp

FULL LENGTH ARTICLE

Endosomal trafficking defects in patient cells with *KIAA1109* biallelic variants

Megan S. Kane [a,*], Callie J. Diamonstein [a], Natalie Hauser [a], John F. Deeken [a,b], John E. Niederhuber [a,c,d], Thierry Vilboux [a,]**

[a] *Inova Translational Medicine Institute, Inova Health System, Fairfax, VA, United States*
[b] *Department of Medicine, Virginia Commonwealth University, Richmond, VA, United States*
[c] *Department of Public Health Sciences, University of Virginia School of Medicine, Charlottesville, VA, United States*
[d] *Department of Oncology and Surgery, Johns Hopkins University School of Medicine, Baltimore, MD, United States*

Received 10 August 2018; accepted 27 December 2018
Available online 7 January 2019

KEYWORDS
Cilia;
Endocytosis;
KIAA1109;
Neurological malformation;
Vesicular trafficking

Abstract The uncharacterized gene *KIAA1109* has recently been associated with a congenital neurological malformation disorder that variably presents with arthrogryposis, craniofacial and/or cardiac abnormalities. We have identified two additional patients with compound heterozygous *KIAA1109* variants presenting with the same neurological malformations. The mechanism whereby KIAA1109 loss of function causes this spectrum of disorders was the primary focus of our studies. We hypothesized that *KIAA1109* function could be conserved relative to the fly gene *tweek* and examined endocytosis and endosome recycling in patient fibroblasts. Furthermore, we examined the structure of the cytoskeleton and cilia based on functional overlap with endocytosis and several known etiologies for neuronal migration disorders. Utilizing primary dermal fibroblasts from one patient and a healthy donor, we performed immunofluorescence and endocytosis assays to examine the endosomal, cytoskeletal, and ciliary cellular phenotypes. We found notable abnormalities in endosomal trafficking and endosome recycling pathways. We also observed changes in the actin cytoskeleton and cilia structural dynamics. We conclude that the function of *KIAA1109* in humans may indeed overlap with the function of the *Drosophila* ortholog, resulting in perturbations to endosomal trafficking and the actin cytoskeleton. These alterations have ripple effects, altering many pathways that are critical for proper neuronal migration and embryonic development.

* Corresponding author.
** Corresponding author.
E-mail addresses: megan.kane@inova.org (M.S. Kane), Thierry.vilboux@inova.org (T. Vilboux).
Peer review under responsibility of Chongqing Medical University.

https://doi.org/10.1016/j.gendis.2018.12.004

Introduction

Clinical implementation of next generation sequencing has led to an increase in the rate of identification of candidate genes for rare genetic disorders. However, many of these novel disease-associated genes may be functionally uncharacterized. These emerging genotype-phenotype associations present a unique opportunity to study uncharacterized genes, elucidating the functional role of the gene products in both the healthy and disease state. By studying these rare conditions, we are able to expand our knowledge of basic biology and gain insight into the pathologic mechanism of disease.

To this end, we have identified two brothers from non-consanguineous African-American parents with novel variants in the gene *KIAA1109* and have performed functional studies to begin to understand the cellular etiology of disease. The patients presented with neurologic malformations, severe developmental delay and hypotonia requiring assisted ventilation and feeding by gastronomy tube. A large cohort of patients with *KIAA1109* variants was recently published,[1] all with marked phenotypic similarities to the patients reported herein.

The human *KIAA1109* gene localizes to the long arm of chromosome 4 and encodes a protein of 5005 amino acids with a predicted molecular mass of 555.5 kDa. Aside from association with the newly described arthrogryposis and neurological malformation syndrome,[1] this gene has been associated with connective tissue cancers and is thought to function in the regulation of epithelial growth and differentiation (NCBI). Genome-wide association studies have also linked this locus to inflammatory conditions affecting the gastrointestinal tract, type I diabetes and rheumatoid arthritis,[2–6] though this may be due to *KIAA1109* linkage with genes *IL2* and *IL21*. Animal models of *KIAA1109* orthologues have implicated those proteins in spermatogenesis and adipocyte differentiation,[7] epithelial differentiation and inhibition of tumor development,[8] and synaptic vesicle recycling.[9] However, the function of the human protein and its proposed relation to a severe neurologic developmental disorder with joint contractures remains to be elucidated.

Functional studies of animal models have begun to elucidate the role of KIAA1109 orthologues. Knockout of the *Drosophila melanogaster* gene *tweek* results in a neurologic defect consistent with abnormal synaptic vesicle recycling and decreased endocytosis at the presynaptic neuron.[9] Tweek protein has also been shown to play a role in neuromuscular junction morphology by affecting the function of Wiscott-Aldrich syndrome protein (WSP) and Nervous Wreck (NWK).[10] Collectively, these studies connect tweek protein function to neurologic function within both the central and peripheral nervous systems.

Endocytosis and recycling of endocytic vesicles are vital for cellular membrane homeostasis and must be appropriately balanced. Upon internalization, endocytic vesicles must be sorted to their appropriate destination. For example, some internalized receptors must be trafficked to an acidic compartment to mediate ligand release; others will be shuttled back to the plasma membrane. Regulation of plasma membrane dynamics and lipid composition via endocytosis and endosomal recycling play a key role in many cellular processes including cell migration and signal transduction.[11] Endocytosis occurs via multiple mechanisms, but commonly converge on trafficking to an early endosome followed by the sorting endosome where cargoes are selected for one of three potential destinations: lysosomal degradation via Rab7-mediated transport, Rab4-dependent rapid recycling to the plasma membrane, or slower recycling through the recycling endosome and ultimately through Rab11- or Rab8-mediated transport to the plasma membrane.[11,12] The precise mechanisms determining which cargoes will be sorted to which destination are complex and employ a wide range of accessory proteins.

The mechanisms underlying multiple neurologic malformations have been elucidated by genetic and molecular analyses. Mutations in genes encoding microtubule (MT) proteins, MT-regulatory or MT-based motor proteins, a transcription factor, a cyclin-dependent kinase, very low density lipoprotein receptor, and multiple actin proteins have been associated with neurologic disorders and malformations including lissencephaly, polymicrogyria, and microcephaly.[13,14] Within each sub-type of neurologic malformation, multiple genes mapping to different predicted functional pathways have been implicated. It is of interest that a significant number of these genes map to the cytoskeleton and transmembrane signaling pathways, either directly or indirectly through protein glycosylation, mTOR signaling, or ciliary function.[14] Indeed, the ciliopathies are known to present with a number of neurologic malformations including the molar tooth sign, Dandy Walker malformation, and agenesis of the corpus callosum.[15]

In this manuscript, we describe the clinical presentation and molecular findings for two male siblings with *KIAA1109* variants. We describe preliminary functional studies performed on fibroblasts isolated from the proband in an attempt to unravel the mechanism of disease due to *KIAA1109* deficiency.

Methods

Patient recruitment

Patients A and B and their parents were enrolled in the Inova Institution Review Board (IRB# 15-1816) and Western Institutional Review Board (WIRB #20121680) approved protocol "The Incidence and Burden of Congenital Anomalies, Genetic Disorders and Genetic Suspicion in Neonatal and Pediatric

Patients." Informed consent for participation in this research study as well as release for publication of photographs were obtained at the time of subject enrollment.

Cell culture

Primary fibroblasts were isolated from skin biopsy obtained during gastronomy tube placement surgery for patient B. Primary dermal fibroblasts were obtained by enzymatic digest of the biopsy with collagenase as previously described.[16] Cells were maintained in high glucose (4.5 g/L) DMEM (ThermoFisher Scientific, 11965118) supplemented with 15% heat-inactivated fetal bovine serum (ThermoFisher Scientific, 16140071) and 1% of antibiotic/antimycotic (ThermoFisher Scientific, 11965118) and incubated at 37 °C in 5% CO_2. Control cells, PCS-201-010 (PCS Ctl), were obtained from ATCC; lot # 61779201 was obtained from a neonatal foreskin sample donated from a healthy African American male.

KIAA1109 transcript analysis

Patient and control fibroblast lines were grown in 10 cm round dishes and sub-confluent cultures were collected in PBS, then transferred to PaxGene (PreAnalytiX) tubes for total RNA isolation with the QiaSymphony (Qiagen) using Ambion MagMax RNA Isolation kit (Thermo Fisher Scientific) per manufacturer's protocol. RNA was then further purified and concentrated using a ZR-96 RNA Clean & Concentrator kit (Thermo Fisher Scientific) prior to quantification by NanoDrop spectrophotometry (Thermo Fisher Scientific). A total of 200 ng total RNA was reverse transcribed using the VILO SuperScript cDNA synthesis kit (Thermo Fisher Scientific). Quantitative real time PCR was performed with 200 ng of cDNA, using Power SYBR Green master mix (Thermo Fisher Scientific) and two sets of primers spanning exons 20-21 in *KIAA1109* mRNA (primer sequences available upon request). Thermal cycling was performed on a BioRad CFX96 and expression analysis was performed with the CFX Manager software (BioRad).

Sequencing of cDNA was performed with four primer sets, each set spanned a unique exon range of either 5-7, 5-9, 5-10 or 6-7 (primer sequences available upon request) to determine allele specific expression and assess splicing. PCR was performed with AmpliTaq Gold 360 reagents (Thermo Fisher Scientific) with a touchdown thermal cycling program with annealing temperature ranging from 61 °C to 51 °C followed by ExoSap (Thermo Fisher Scientific) purification and BigDye Terminator v3.1 Cycle Sequencing Kit for Sanger sequencing. Samples were run on an Applied Biosystems 3500xL genetic analyzer (Thermo Fisher Scientific) per the manufacturer's protocol. Sequences were analyzed using Sequencher software (GeneCodes).

Dextran endocytosis assay

Dextran labeling experiments utilized fixable Dextran, Alexa Fluor™ 555 (Thermo Fisher Scientific, D34679) at a 1 mg/mL final concentration. Cells were incubated with the dextran in serum-rich media for 2.5 h to saturate trafficking pathways. The cells were then washed four times with serum-rich media without dextran, then incubated for 0, 5 or 10 min with serum-rich media to "chase" the dextran label inside the cells. Unstained cells were grown in serum-rich media and subjected to similar washes. Cells were fixed in 4% paraformaldehyde (Electron Microscopy Sciences, 15710) for 20 min, and then washed in phosphate-buffered saline (PBS) prior to immunofluorescence staining.

Ciliogenesis and resorption

To induce cilia formation, cells were grown directly on sterile round cover glass in a 24-well dish. Within 18—24 h after plating in serum-rich media, the cells were washed twice with PBS, then cultured for an additional 48 h in serum-free DMEM. To induce cilia resorption, the media was replaced with serum-rich media for the indicated time points. Cells were fixed with ice-cold methanol for 20 min prior to immunostaining for ciliary proteins. Experiments were repeated in triplicate with >100 cells scored for ciliation at each time point.

Immunofluorescence

Immunofluorescence experiments utilized 4% bovine serum albumin (BSA, Sigma—Aldrich, A7030) in PBS as blocking reagent and antibody diluent. Where necessary, fixed cells were permeabilized with 0.1% Triton-X 100 in PBS prior to blocking. Dextran labeled cells were not permeabilized, but utilized 0.05M glycine in the blocking media. Actin filaments were labeled with Alexa-647 conjugated Phalloidin dyes (ThermoFisher Scientific, A22287) per the manufacturer protocol. Primary antibodies used were anti-Alpha tubulin (1:500, Abcam ab7291), anti-ARL13B (1:250, ProteinTech 17711-1-AP), anti-gamma tubulin (1:250, Sigma—Aldrich T5326), anti-EEA1 (1:200, SantaCruz Biotechnology sc-6414), anti-LAMP3 (1:200, ThermoFisher Scientific, MA1-35272), anti-Rab9 (1:500, ThermoFisher Scientific, MA3-067), anti-Rab4 (1:250, ThermoFisher Scientific, PA3-912), anti-Rab11a (1:250, SantaCruz Biotechnology sc-166912), and anti-Rab7 (1:100, ThermoFisher Scientific, PA5-52369). Secondary antibodies used were donkey anti-rabbit, anti-mouse or anti-goat and conjugated to AlexaFluor fluorophores (ThermoFisher Scientific, 1:1000 dilution). Primary and secondary antibodies were diluted in 4% BSA in PBS. DNA counterstaining utilized Hoechst33342 dye (ThermoFisher Scientific, H1399), diluted 1:5000 in PBS.

Cellular imaging and analysis

Stained cells were imaged on a Zeiss LSM700 confocal microscope at 20x magnification with uniform imaging conditions for patient and control cells. Z-stack images spanning the full range of fluorescence signal with 1 μm slices were processed to 2D maximum intensity projections prior to image analysis. Cilia analysis was performed by manual counting of ciliated and non-ciliated cells and length measurement in FIJI.[17] Cilia were defined as ARL13B positive structures adjacent to one or more gamma-tubulin positive puncta with a minimum length of 1 μm. Images of the endosomal pathway and dextran assay were analyzed using Cell Profiler[18] with customized pipelines developed

and adjusted to the unique parameters of each set of stains utilized (see supplemental methods for details of Cell Profiler pipelines). In brief, each pipeline imported color images for each channel, converted the images to grayscale then identified primary objects based on the stain utilized for each specific image. Nuclei were defined by Hoechst staining, endosomal compartments by their respective stains and Dextran-positive puncta by dextran fluorescence. Where utilized, actin and alpha-tubulin were used to define the borders for secondary objects, the cell body, based on the primary nuclei. When not available, cell borders were defined based on a lower threshold of endosomal marker stains and these parameters were adjusted specific to each staining experiment, trained on control cell images and used consistently for both patient and control images. Multiple fields of cells were analyzed per cell line for each experiment, resulting in automated analysis of hundreds of cells (200-500 cells per line per experiment), with similar cell counts between control and patient cells within each experiment.

Statistical analysis

Statistical analyses utilized the Student's t-test with two-tailed, two-sample heteroscedastic parameters. Significance was determined based on $p < 0.025$. Where shown in the figures, error bars represent the standard error of the measurement average.

Results

Case report

The older male sibling, "patient A," was a product of the fourth pregnancy of a healthy, 34-year-old mother (Fig. 1A). The parents had a healthy older daughter (age 7 years at time of birth of patient A) and a history of two first trimester miscarriages. Routine prenatal anatomy ultrasound revealed a brain malformation, and subsequent fetal MRI documented underdevelopment of the brain stem and lack of normal gyria. The infant was born at full term (39 weeks gestational age) via C-section, at ~3rd percentile for weight. After birth, diffuse hypotonia and congenital cataracts were noted. Joint contractures were not present. Postnatal brain MRI (at less than one month of age) demonstrated extensive cerebellar dysplasia, a hypoplastic midbrain, abnormal segmentation of the pons and medulla, extensive cortical dysplasia/polymicrogyria in the sylvian regions, severe hypogenesis of the corpus callosum, small abnormal lens, and hypoplastic ring of C1 with resulting mild upper cervical stenosis. By about 2 months of age, failure to thrive was noted. At 4 months of age, he developed seizures (EEG showed focal seizures in left frontal temporal region) with hypsarrhythmia noted at 6.5 months. At 7 months of age, the patient was found to have severe oropharyngeal dysphagia after a choking episode that led to aspiration, respiratory distress and apnea. Subsequently at 9.5 months of age, a tracheostomy and g-tube were placed for respiratory failure and poor feeding, respectively. Currently, at 23 months of age, the patient remains with a tracheostomy and is g-tube dependent for nutrition with a profound lack of development (Fig. 1B). He has been frequently hospitalized due to complications from tracheostomy and/or viral illnesses.

The younger male sibling, "patient B," was born via C-section at 35 weeks 5 days gestation due to maternal pre-eclampsia. There were no fetal concerns during the pregnancy. Patient B was transferred to the NICU soon after birth due to hypothermia. On initial examination, hypertonia with clenched fists and congenital cataracts were noted. Joint contractures were not present in patient B. Head ultrasound at 10 days was abnormal, showing absent corpus callosum, ventriculomegaly and markedly irregular appearance of the lateral ventricles. Brain MRI on the same day demonstrated numerous developmental anomalies, including polymicrogyria, enlarged ventricles secondary to white matter volume loss, inferior vermin hypoplasia, pontine hypoplasia, congenital cataracts, and small optic nerves (Fig. 1D and E).

Patient B showed poor feeding with aspiration due to severe pharyngeal dysphagia by 18 days of life. He developed seizures at 61 days. After being hospitalized at 78 days for multiple apneic episodes, a tracheostomy and g-tube were placed due to respiratory failure and persistent dependence on artificial feeding methods (Fig. 1C). During this surgical procedure, a small biopsy of skin was collected to propagate primary fibroblasts for functional studies. At 12 months of age at last contact, patient B is profoundly developmentally delayed and requires extensive medical attention.

Differential diagnoses for these patients included potential neuronal migration disorders and atypical ciliopathy presentation. However, clinical exome sequencing by GeneDX (Gaithersburg, MD) identified only one pair of compound heterozygous variants with proper segregation in both affected brothers and their parents. These variants in the gene *KIAA1109* were classified as variants of uncertain significance. The paternally inherited allele encoded for a premature termination codon (NM_015312.3:c.13123C>T; p.(Arg4375*)); to date, this nonsense variant is the closest to the C terminus end of the protein described. The maternally inherited allele encoded two missense variants in *cis* (NM_015312.3:c.648T>G; p.(Asn216Lys) and NM_015312.3:c.683A>G; p.(Asp228Gly)). The p.(Asn216Lys) variant is predicted to be deleterious by SIFT (Deleterious (score: 0)[19]), MutationTaster (Disease causing (prob: 1)[20]) and PolyPhen2 (Probably Damaging (HumVar score: 0.986)[21]). The p.(Asn228Gly) is predicted to be deleterious by SIFT (Deleterious (score: 0)[19]), MutationTaster (Disease causing (prob: 1)[20]) and PolyPhen2 (Possibly Damaging (HumVar score: 0.612)[21]). Neither allele affects any known or predicted domains in KIAA1109 protein. Splicing prediction tools generated conflicting results as to whether the maternal variants could alter splicing, but at least one predicted alternative splice site results in a frameshift (Table S1).

Functional studies

Quantitative real-time PCR on total mRNA extracted from fibroblasts showed an approximately 60% reduction in *KIAA1109* transcript levels in the patient relative to control

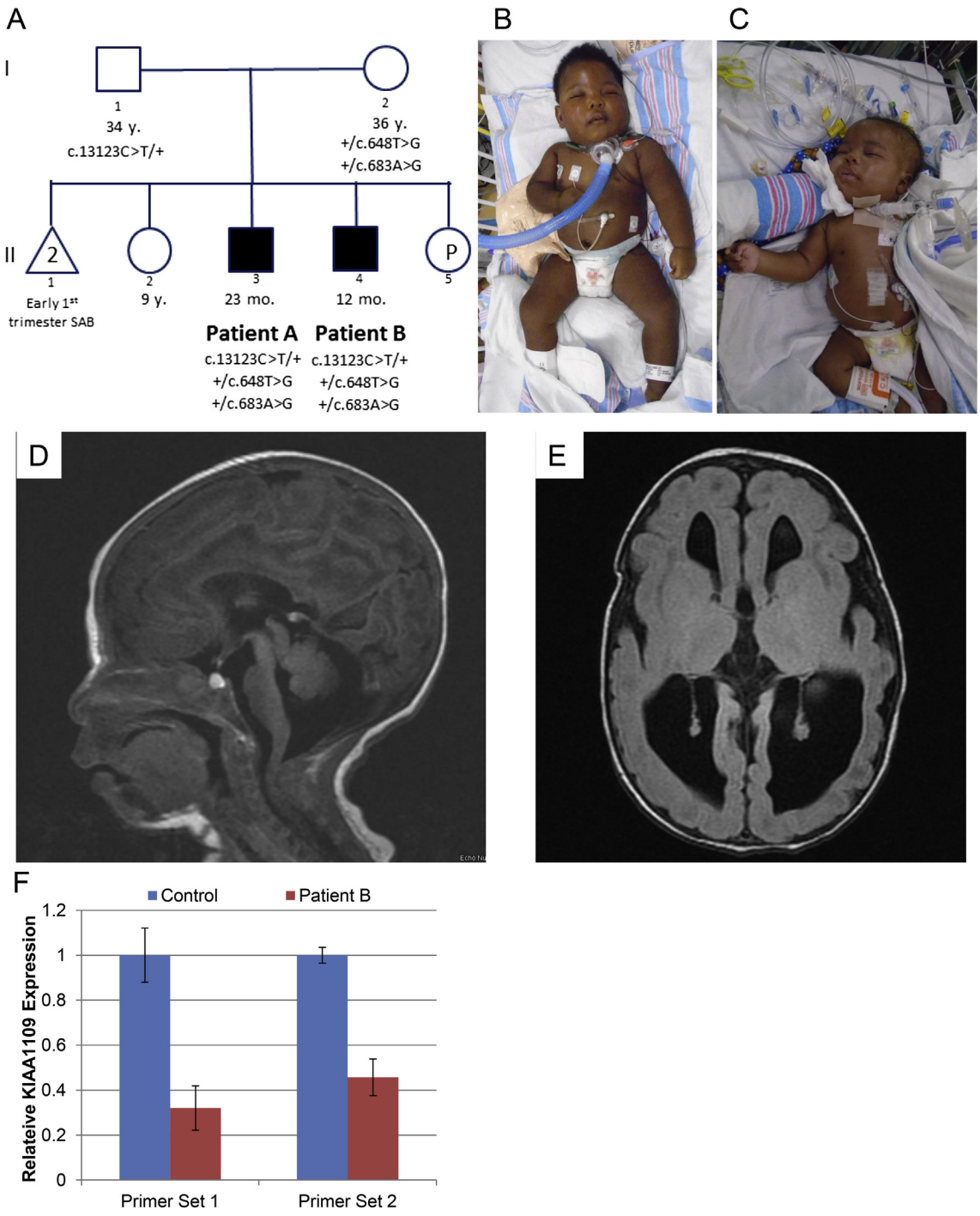

Fig. 1 Clinical description of patients A and B. The family pedigree (A) shows the segregation of the paternal and maternally inherited variants in *KIAA1109* (NM_015312.3 cDNA coordinates given). Genotyping is unavailable for individuals II-2 and II-5. Patient A at 18 months of age (B) and patient B at 4 months of age (C). Sagittal (D) and axial (E) views of brain MRIs of patient B show polymicrogyria, vermin and pontine hypoplasia as well as enlarged ventricles.

(Fig. 1F). Expression variability across technical replicates ranged from 12.1% in control to 3.5% in patient samples for primer set 1, and 9.8% in control to 8.2% in patient samples for primer set 2. Overall, this averages to a range of 30—50% residual mRNA expression in the proband. Sequencing of the residual *KIAA1109* transcripts across the region encoding the maternal missense variants showed stable expression from both the maternal and paternal alleles (Figure S1). Cloning and colony sequencing of regions flanking both the paternal and maternal variant sites from primary fibroblast cDNA showed roughly 20% of the clones sequenced encoded the paternal variant and 72% of the clones encoded the maternal variant (Table 1). The cloned constructs (spanning exons 5-9 and 5-10) show no evidence

of aberrant splicing flanking the maternal variants. Taken together, these data suggest that the paternal allele encodes a destabilized mRNA which partially evades nonsense mediated decay (NMD), contributing to reduced total *KIAA1109* transcript levels. We conclude that any mis-spliced mRNA from the maternal allele is efficiently targeted for NMD and thus is undetected by our methods.

Confirmation of two deleterious alleles in *KIAA1109* and review of the literature suggested endocytosis could be affected in these patients.[9] Analysis of the endocytic pathway by immunofluorescence showed an increase in independent foci with both the early endosome marker EEA1 and lysosomal protein LAMP3 (Fig. 2A, B and C). Staining for late endosome marker Rab9 showed no significant differences between cell types (Fig. 2D). These steady-state images suggested a defect in early endocytic trafficking with an increase in lysosomes, but with no effect on late endosomes.

Endosomal trafficking was more closely examined by staining for endosomal recycling markers Rab4 and Rab11 as well as lysosomal trafficking protein Rab7. Rab4, a key protein in fast endosome recycling, showed an increase in average punctum size in patient cells (Fig. 3A i-ii and B) with no significant difference in overall puncta count per cell (data not shown). Rab11, a marker for slow endosome recycling, showed a decrease in punctum size in patient cells (Fig. 3A i-ii and C) with a modest increase in number of puncta per cell *versus* control ($p = 0.029$, data not shown). Rab7, a key factor in transporting endocytosed cargo to the late endosome and lysosome, showed significantly more puncta and larger punctum size in patient cells *versus* control cells (Fig. 3A iii-iv, D and E). Taken together, these data indicate an increase in trafficking toward lysosomal degradation in *KIAA1109* mutant cells with a defect in trafficking through the slow endosomal recycling path.

Endocytosis was further studied in patient and control cells by labeling with fluorescent dextran and examining the ability of the cells to traffic endocytosed dextran through the early and late endosomes as well as recycling endosomes. After saturating the endocytic pathway with fluorescent dextran, cells were fixed after 5 and 10 min in dextran-free media. The two "chase" time points were selected to observe trafficking of the endocytosed material within patient cells relative to the endocytic compartments. We observed a brighter overall dextran signal in patient cells at both 5 and 10 min time points of the assay (Fig. 4A). Furthermore, we observed more correlation of the dextran with early endosomal marker EEA1 in patient and control cells at both 5 and 10 min (Fig. 4B). Representative micrographs for the 5 min chase time point are shown in Fig. 4C for all endosomal markers assayed in both Patient B (Pt. B) and control (PCS Ctl) cells.

Correlation between the dextran and various endosomal markers was examined at 0, 5 and 10 min. Surprisingly, at both 0 and 5 min chase, dextran showed an increased correlation with Rab11 in patient cells (Fig. 4D), despite the decrease in Rab11 puncta size in these cells (Fig. 3C). An increase in correlation for patient cells was also seen for the fast recycling compartment initially (Rab4, Fig. 4E), but not at later time points. Late endosomal marker Rab9 showed decreased correlation in control cells at 0 min, slightly increased correlation at 5 min, but equivalent correlation at 10 min. Rab7 showed increased correlation in patient cells only at the initial time point of the assay, with no significant differences between patient and control at 5 or 10 min (Fig. 4G). These data suggest a defect in vesicular trafficking in patient cells *vs*. control, with an accumulation of dextran in the patient cells and a higher amount of dextran in all endocytic compartments initially, with prolonged retention in the early endosome.

As neuronal migration disorders and ciliopathies were initially considered in the differential diagnosis, we considered if the putative role of KIAA1109 protein in endocytosis may also intersect with the function of the cytoskeleton or cilia. Vesicular trafficking, particularly Rab11 slow-endosome recycling, is dependent upon the actin cytoskeleton.[22] Likewise, endocytosis and vesicle recycling is critical for maintenance of the ciliary pocket and ciliary membrane composition.[23,24] Vesicle trafficking is also critical for formation of the cilia, with Rab11 playing a prominent role in early cargo delivery.[25]

We examined the actin cytoskeleton in the primary fibroblasts from patient B. Staining of actin filaments with phalloidin consistently resulted in apparently weaker signals in the patient cells *versus* control fibroblasts (Fig. 5A i-ii), with a qualitative decrease in actin stress-fiber prominence. This was quantified by automated image analysis, confirming an increase in distinct actin fibers and overall staining intensity in control cells relative to patient B (Figure S2 A and B). Alpha tubulin staining showed no

Table 1 Results of cloning and sequencing of the indicated cDNA regions from control and Patient B primary fibroblasts.

	Count WT	Count Var	Count misspliced	Count Total Clones	% WT	% Var
Paternal Variant Site: NM_015312.3:c.13123C>T						
Control Fibroblasts	113	0	1	114	99.1%	0.9%
Patient B	90	22	0	112	80.4%	19.6%
Maternal Variant Site 1: NM_015312.3:c.648T>G						
Control Fibroblasts	110	0	0	110	100.0%	0.0%
Patient B	33	83	0	116	28.4%	71.6%
Maternal Variant Site 2: NM_015312.3:c.683A>G						
Control Fibroblasts	113	0	0	113	100.0%	0.0%
Patient B	33	83	0	116	28.4%	71.6%

Results of cloning and sequencing the indicated cDNA regions from control and Patient B primary fibroblasts. WT = wildtype; Var = variant.

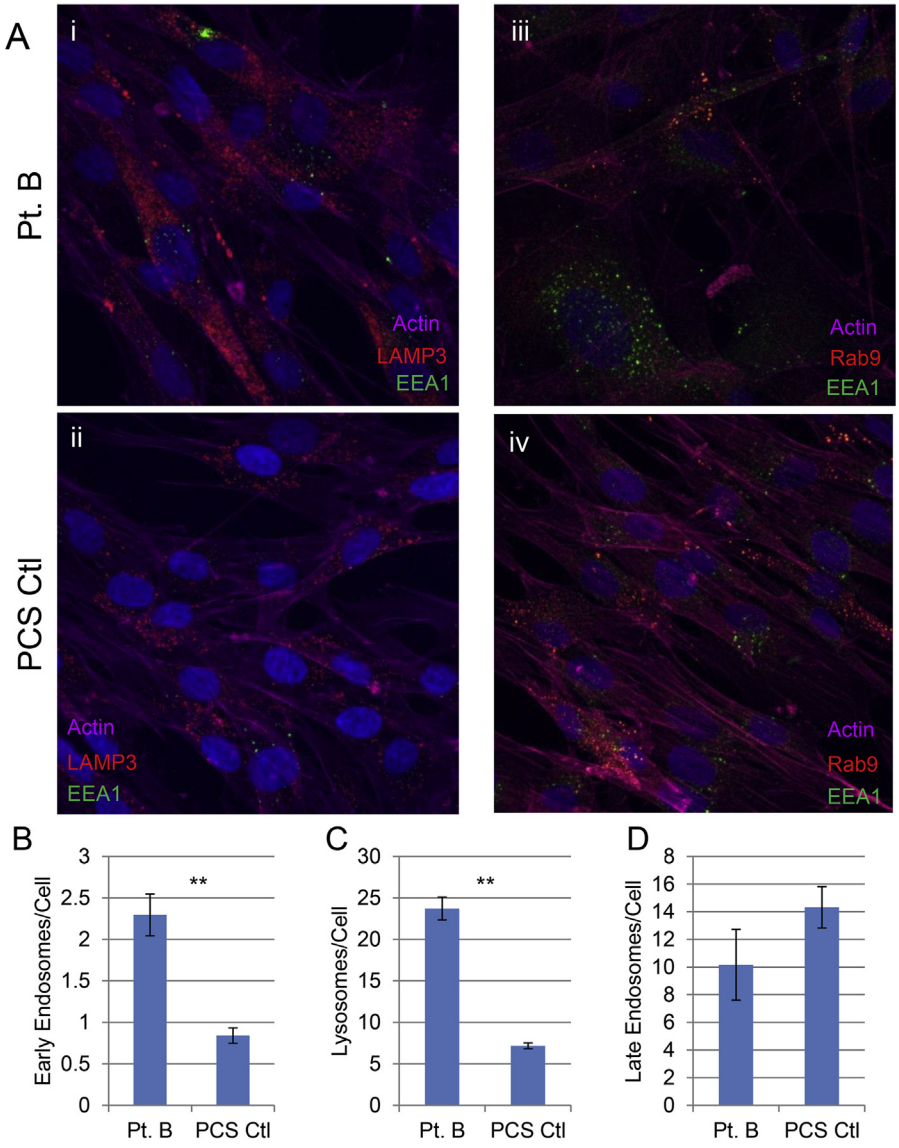

Fig. 2 Analysis of endosomal pathway at steady state in fibroblasts. Immunostaining for actin (magenta), lysosomal protein LAMP3 (red), and early endosome protein EEA1 (green) in patient B (Pt. B) and control (PCS Ctl) cells (A i-ii). Immunofluorescence imaging of patient B (Pt. B) and control (PCS Ctl) cells stained for actin (magenta), late endosome maker Rab9 (red), and early endosome protein EEA1 (green) (A iii-iv). Quantification of the average number of early endosomes ($p = 8.49E-8$) (B), lysosomes ($p = 7.09E-28$) (C), and late endosomes (not significantly different) (D) in fixed cell images from Pt. B and PCS Ctl cells. DNA counterstaining in blue (Hoechst). Error bars represent SEM. ** $p < 0.01$ * $= p < 0.025$.

remarkable qualitative differences in Patient B and control cells (Fig. 5A iii-iv).

We next subjected the patient cells to a ciliogenesis assay with ciliary resorption. We found no significant differences in the frequency of ciliated cells after 48 h of serum starvation (Fig. 5B), but observed a more rapid resorption of the cilia in patient cells upon reentry into the cell cycle (Fig. 5B, +FBS 2hr time point, $p < 0.01$). Furthermore, the average cilium length in patient cells was 4.6 μm *versus* 3.7 μm in control cells (Fig. 5C, $p < 0.01$). These data suggest the patient cells can form cilia, but show an increase in cilia dynamics leading to longer cilia and more rapid resorption. Whether or not the patient's cilia are functionally compromised remains to be tested.

Discussion

In this study, we reported two male siblings with biallelic *KIAA1109* variants, with phenotypic similarities to previously reported cases.[1] These siblings carry two unreported variant alleles in *KIAA1109*, expanding the genotypes associated with this neurological and developmental disorder. Our patients present with similar brain malformations to the 13 previously reported patients as well as hypotonia and severe developmental delay, and congenital cataracts. There are, however, notable phenotypic differences to the published cohort of patients. Both patient A and B lack joint contractures or club foot as well as cardiac anomalies, which were seen in at least half of the

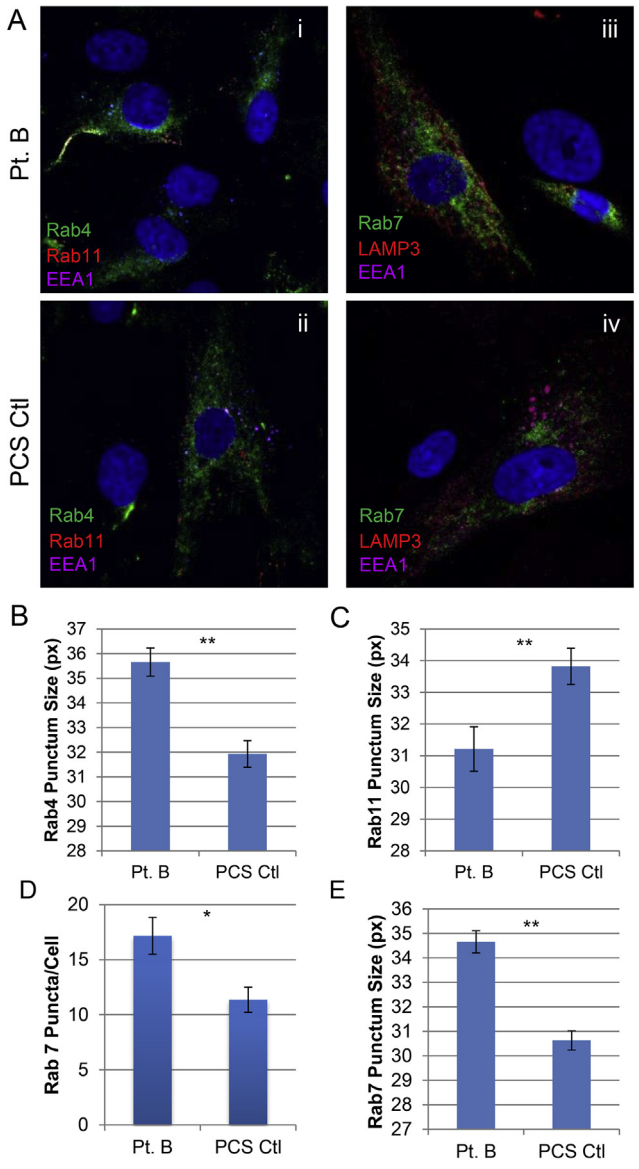

Fig. 3 Endosomal trafficking and recycling pathways. Immunofluorescence staining for fast (Rab4, green) and slow (Rab11, red) endosome recycling components with early endosome marker EEA1 (magenta) in patient B (Pt. B) and control (PCS Ctl) cells (A i-ii) or lysosomal trafficking (Rab7, green) and lysosomal protein LAMP3 (red) with EEA1 (magenta) in Pt. B and PCS Ctl cells (A iii-iv). Quantification of punctum size (in pixels, px) for Rab4 fast recycling endosomes ($p = 2.0E\text{-}6$) (B) and Rab11 slow recycling endosomes ($p = 0.004$) (C) from steady state cells. Quantification of the Rab7 lysosome trafficking puncta count per cell ($p = 0.0111$) (D) and size in pixels ($p = 1.74E\text{-}13$) (E) also in steady state cells. Error bars represent SEM. ** $= p < 0.01$ * $= p < 0.025$.

previously reported cases.[1] Less frequent issues involving craniofacial development are also absent in our two patients. It should be noted that the paternally inherited nonsense mutation in our patients occurs more 3′ than other reported variants, potentially resulting in increased residual function from this specific allele. The maternally inherited missense variants are in a more 5′ region of the mRNA, distal to the other reported missense variants that are more centrally clustered in the coding region of *KIAA1109*. It is also unclear whether one or both of the maternally inherited missense variants contribute to the KIAA1109-deficiency phenotype. Both variants are absent from public databases (dbSNP, gnomAD, NHLBI ESP, etc.) and both are predicted to alter the protein function. Both paternal and maternal alleles appear to encode partially unstable mRNA, resulting in only 40% residual transcript levels in the patient fibroblasts relative to control cells, with biallelic expression at the transcript level (Figure S1). Cloning showed that 20% of the stable transcripts contained the paternal variant and 70% contained the maternal variants (Table 1). Given the persistence of some mRNA encoding the paternal variant, we propose that the maternal allele may also be destabilized, though the vast majority of residual mRNA arises from the maternally inherited allele. The paternal allele may partially evade nonsense mediated decay due to exon-junction proximity.[26] The second variant in the maternal allele (c.683A>G) was predicted by Human Splicing Finder[27] to alter mRNA splicing (Table S1, 3′ variant), resulting in a frameshift and premature termination, though we did not observe any evidence of exon skipping (Table 1).It is possible that any misspliced mRNAs are efficiently targeted for NMD. Ultimately, whether one or both maternal variants contribute to the patients' phenotype is unclear. Further efforts to delineate the degree of functional impact of the known *KIAA1109* missense variants should be considered to expand our understanding of the genotype-phenotype correlation in these patients.

The presence of null allele variants in public database such as gnomAD (Probability of loss-of-function intolerance (pLI) = 0.00) suggest that *KIAA1109* is tolerant to heterozygote loss of function variant and therefore haploinsufficiency or simple reduction of mRNA level of *KIAA1109* may not be sufficient to explain patient phenotype.

In light of this cohort of patients with biallelic *KIAA1109* variants, we sought to address how pathogenic variants in *KIAA1109* induce abnormal molecular and cellular functions responsible for the phenotype observed in these patients. We approached the potential mechanism of disease in two ways. First, we considered putative conserved KIAA1109 protein function from what is known from animal models, specifically vesicle recycling and endocytosis. Second, we considered the phenotypic overlap with disorders of neuronal migration, which suggested the cytoskeleton or even cilia might be impacted in the patient cells. For this, we examined these cellular processes in our patient-derived dermal fibroblasts.

Our analysis of endocytosis and trafficking showed differences between control and patient cells. The increase of early endosomes and lysosomes suggest a defect in trafficking through the early endosome and a potential upregulation of trafficking to the lysosome. The lysosome may or may not have compromised function, resulting in an abundance of the lysosome membrane protein LAMP3. The localization of endocytosed dextran with multiple endosomal trafficking components shows there is some retained trafficking functionality in the patient cells, but accumulation of a specific marker for the early endosome and

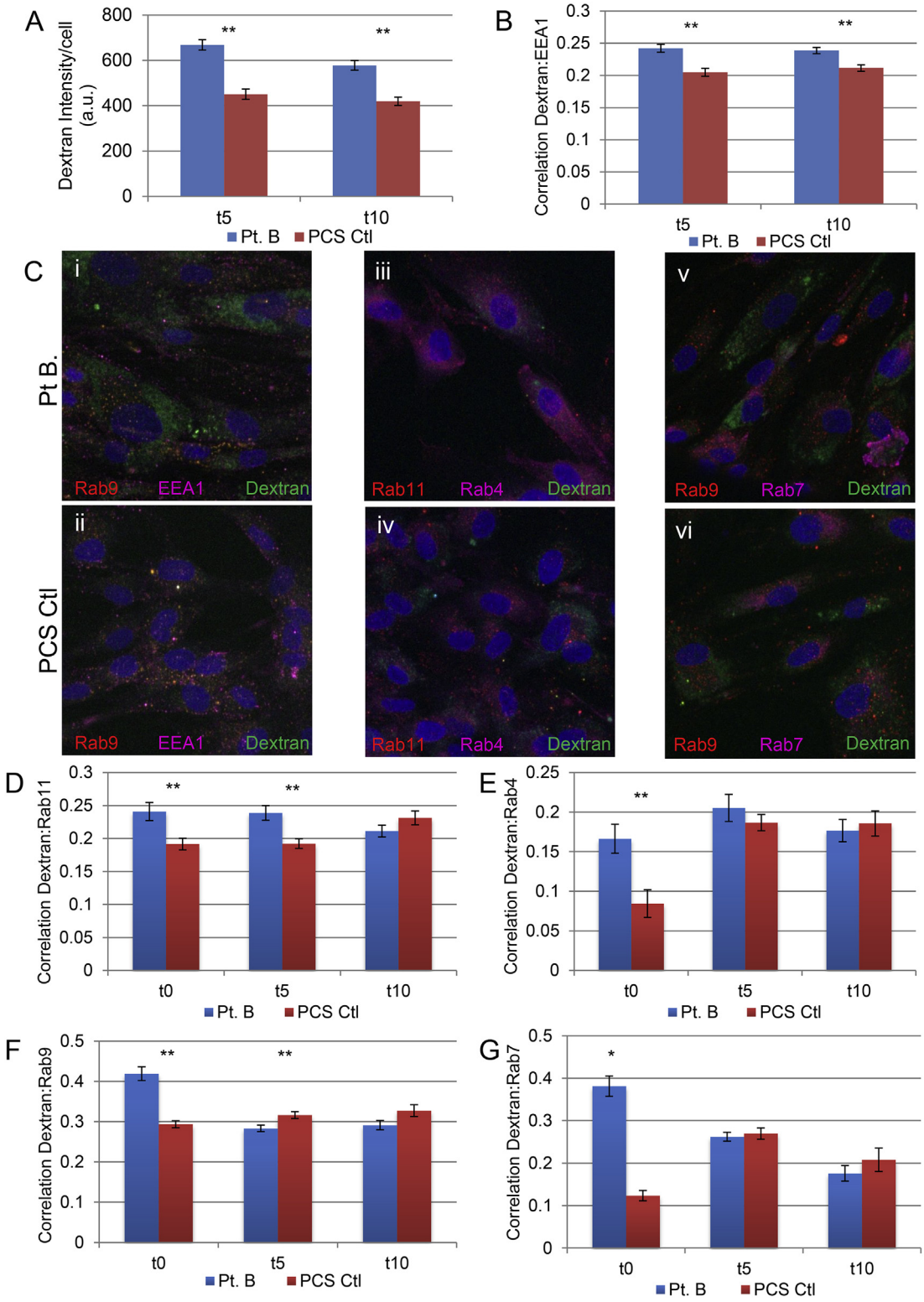

Fig. 4 Dextran endocytosis trafficking assay. Dextran overall intensity within the cell at 5 and 10 min of dextran chase in patient B (Pt. B) and control (PCS Ctl) cells (A). Correlation of dextran signal with EEA1 signal in cells at 5 and 10 min of dextran chase in Pt. B and PCS Ctl (B). Representative micrographs of immunofluorescence staining of dextran (green) labeled Pt. B and PCS Ctl cells at 5 min with various endosomal markers: Rab9 late endosomes (red) and EEA1 early endosomes (magenta) (C i-ii), Rab11 fast- (red) and Rab4 slow-recycling endosomes (C iii-iv), and Rab9 late endosomes (red) with Rab7 lysosomal targeted vesicles (magenta) (C v-vi). DNA counterstaining in blue (Hoeschst) (C). Correlation of each endosomal and trafficking marker with dextran signal at 0, 5 and 10 min chase time points (t0, t5 and t10, respectively) in dextran assay is shown as indicated in the vertical axis label (D—G). Error bars represent SEM. ** = $p < 0.01$, * = $p < 0.025$.

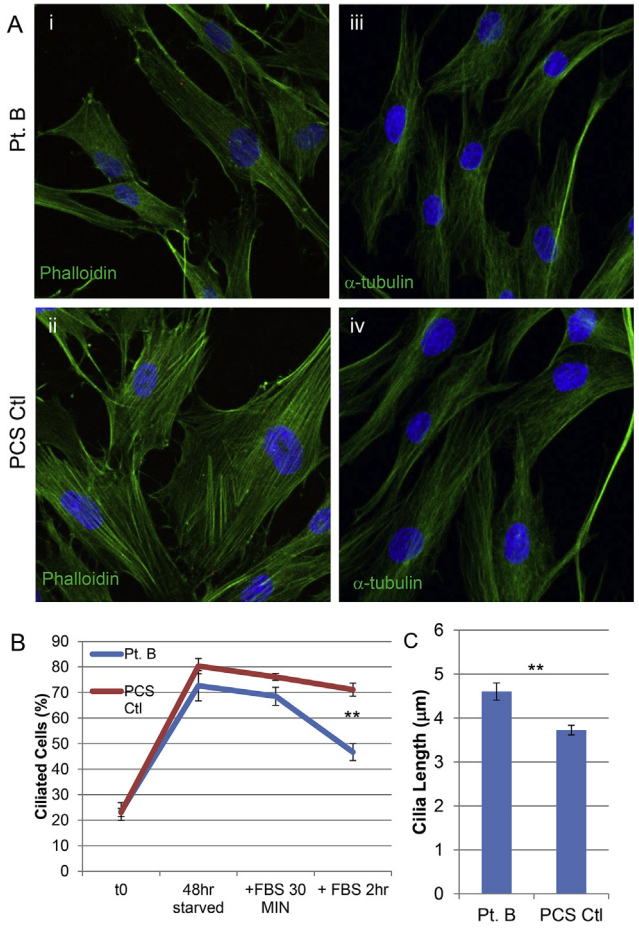

Fig. 5 Analyses of cellular physiology related to the cytoskeleton and cilia. F-actin staining with Phalloidin in Patient B fibroblasts (A i) and PCS control (PCS Ctl) cells (A ii) in green with DNA counterstaining shown in blue (Hoechst). Microtubule staining (green) in Patient (A iii) and PCS Ctl (A iv)) cells with DNA counterstaining in blue. Quantification of the percentage of ciliated cells in Patient B (Pt. B) and control (PCS Ctl) cells during ciliogenesis and resorption (B), ** = $p < 0.01$ only at 2 h of ciliary resorption. Average cilia length after 48 h of serum starvation is increased in patient B's fibroblasts relative to PCS Ctl cells (C), ** = $p < 0.01$. * = $p < 0.025$.

prolonged correlation with this marker suggest a deficiency in efficient trafficking/sorting of endocytosed cargo out of this structure.

In addition, we observed qualitative and quantitative differences in the actin-based cytoskeleton with no observable differences in microtubule structure at steady state. Expression of mutant smooth muscle alpha actin (*ACTA2*) has been shown to reduce the prominence of actin stress fibers in fibroblasts,[28] similar to what we observe in patient B fibroblasts upon staining with phalloidin (Fig. 5). However, loss of beta actin in mouse cells results in an increase in stress fiber formation and a skewing toward F-actin over G-actin[29]; these studies mimic a form of Baraitser-Winter syndrome (BWS), which presents with pachygyria, microcephaly and corpus callosum dysgenesis. Taken together, these findings suggest an appropriate balance of F- and G-actin is critical for cellular function. Our observation introduces the possibility that deficiencies in the actin cytoskeleton are contributing to the pathogenesis of *KIAA1109*-associated neurological disorder and further study on the potential interaction between KIAA1109 protein and actin should be pursued.

We found no significant changes in ciliated cell frequency. However, similar to what we have observed in our patient cells, more rapid ciliary resorption has been seen in a ciliopathy model due to *INPP5E* loss of function.[23] *INPP5E* encodes inositol polyphosphate-5-phosphatase E, which acts to remove the 5-phosphate from poly-phosphorylated inositols, reducing the amount of these lipids in cellular membranes.[30] Thus, it is possible that the *KIAA1109* mutations are affecting ciliary function through a putative conserved role in regulating phosphatidyl-inositol levels, as has been suggested for *tweek*, the *Drosophila* ortholog of *KIAA1109*.[9,10]

We suggest a model whereby KIAA1109 deficiency alters cargo sorting through the early or recycling endosomes, with a pronounced effect on the slow recycling pathway as marked by Rab11-dependent vesicle recycling. This finding is consistent with the proposed function of tweek in synaptic vesicle recycling. This results in an increase cargo load through Rab4 fast recycling endosomes and Rab7-targeting to the lysosome. Generation of branched actin fibers and F-actin are important factors in efficiency cargo sorting and trafficking in the endo-lysosomal pathway, with a well-established role for the WASP-family of proteins (in conjunction with the retromer complex) in cargo sorting, with neuronal WASP (N-WASP) playing a role in vesicular trafficking through the cytoplasm.[31–33] WASP activity in the neuromuscular junction is dependent upon tweek activity.[10] While KIAA1109 has not been shown to interact with any of the WASP family members, it is possible that KIAA1109 loss of function could indirectly influence the function of these proteins and complexes. Tweek mutants have been shown to have an abnormal balance of phosphatidylinositol phosphates (PIPs) ($PI(3,4,5)P_3$, $PI(4,5)P_2$, PI(4)P, etc).[9,10] Members of the WASP family, particularly N-WASP, require $PI(4,5)P_2$ to facilitate actin-nucleation.[33] Whether KIAA1109 can directly interact with any WASP family members or the enzymes involved in PIP synthesis bears further study. Levels of $PI(4,5)P_2$ and conversion into tri- and mono-phosphorylated species are critical factors in endocytosis in conjunction with actin polymerization and dynamics.[34,35]

Regulation of endocytosis and endosome recycling are key processes for ciliary function and stability. Multiple signaling pathways act through receptors on primary cilia and these receptors must be internalized and recycled back to the ciliary pocket to regulate activation of these pathways[24,36,37] Endosome proteins are increasingly shown to play a role in regulating membrane turnover of the primary cilium.[36–38] Multiple Rab proteins, including Rab11, are critical for vesicle targeting and fusion at the ciliary membrane, as well.[23,25] Thus, disruption of endocytosis and endosome recycling is likely to result in disruptions in ciliary function or structure. Our observation of elongated cilia structure and more rapid resorption of cilia suggest an altered homeostatsis of ciliary membranes. Paired with our observations of increased retention of endocytosed material in early endosomes, this suggests a defect in sorting

endocytic vesicles to either be recycled (via fast or slow pathways) or degraded. Rab11-dependent slow recycling of endosomes requires actin-based transport to target recycled cargo back to the appropriate cellular membrane.[22] Thus, disruptions to either the actin cytoskeleton or processes which regulate cargo sorting to Rab11-recycling endosomes can result in similar functional outcomes and potentially similar phenotypes at the organismal and cellular level. Whether the observed endosomal deficiencies are due to altered trafficking along actin filaments or directly via cargo sorting is an open question for further research. Additional studies on KIAA1109 protein function are required to determine if this protein binds to actin filaments or vesicles or both.

Endocytosis, actin cytoskeleton nucleation and stability, and ciliary homeostasis are all interconnected processes, dependent upon each other to maintain cellular homeostasis. While we observe alterations in each of these pathways, it is difficult to predict a single function of KIAA1109 that could result in these cellular phenotypes and cause the systemic and neurological deficits observed in patients with biallelic *KIAA1109* deleterious variants. KIAA1109 protein carries two predicted transmembrane helices in the N-terminus, and *in silico* predictions of conserved functional domains in the C-terminus remain to be functionally validated. Given the size of KIAA1109, it is possible it functions as a scaffolding or docking protein, linking effectors of the endosomal pathway to the actin cytoskeleton for transport and/or cargo sorting. It is possible that the function of KIAA1109 is similar to its ortholog tweek in that it contributes to the regulation of PIP metabolism and conversion among the mono-, bi- and tri-phosphorylated forms of this lipid, which underpins a variety of signaling pathways and cascades.[39,40] Mutations in the WASP family of proteins and their known interactors do present with neurologic phenotypes, however these are generally later onset or degenerative disorders rather than developmental disorders.[41–44] Thus, we predict it is likely that KIAA1109 functions upstream of these complexes, influencing pathways that converge on WASP and retromer-based endosomal sorting while also having ripple effects into broader actin structure, resulting in a more severe neuronal migration disorder phenotype.

In conclusion, we have described clinical findings associated with *KIAA1109* biallelic variants that is in agreement with previous work[1] as well as identified novel missense and nonsense alleles in this uncharacterized gene. We observe altered endocytosis, ciliary dynamics and F-actin structure in patient cells. Each of these interconnected cellular functions likely contributes to the etiology of *KIAA1109*-associated neurological and systemic phenotypes seen in our patients and other reported individuals. Our observations underscore the importance of endocytosis and vesicular trafficking in neurological disorders and have generated additional hypotheses for the cellular function of human KIAA1109.

Conflict of interest

The authors declare no conflicts of interest.

Acknowledgements

The authors would like to thank the patients and their families for participation in this study. We would like to acknowledge Nicole Clemency and John Strang for their excellent technical assistance in establishing and maintaining the patient primary fibroblast cell line. This work would not have been possible without the dedicated clinical staff at Inova Fairfax Hospital, particularly the NICU, PICU, radiology and surgical teams who have contributed to the care of these patients. This work has been supported directly by the Inova Health System.

Appendix A. Supplementary data

Supplementary data to this article can be found online at https://doi.org/10.1016/j.gendis.2018.12.004.

References

1. Gueneau L, Fish RJ, Shamseldin HE, et al. KIAA1109 variants are associated with a severe disorder of brain development and arthrogryposis. *Am J Hum Genet*. 2018;102(1):116–132.
2. Hunt KA, Zhernakova A, Turner G, et al. Newly identified genetic risk variants for celiac disease related to the immune response. *Nat Genet*. 2008;40(4):395–402.
3. Adamovic S, Amundsen SS, Lie BA, et al. Association study of IL2/IL21 and FcgRIIa: significant association with the IL2/IL21 region in Scandinavian coeliac disease families. *Genes Immun*. 2008;9(4):364–367.
4. van Heel DA, Franke L, Hunt KA, et al. A genome-wide association study for celiac disease identifies risk variants in the region harboring IL2 and IL21. *Nat Genet*. 2007;39(7):827–829.
5. Bouzid D, Fourati H, Amouri A, et al. Autoimmune diseases association study with the KIAA1109-IL2-IL21 region in a Tunisian population. *Mol Biol Rep*. 2014;41(11):7133–7139.
6. Glas J, Stallhofer J, Ripke S, et al. Novel genetic risk markers for ulcerative colitis in the IL2/IL21 region are in epistasis with IL23R and suggest a common genetic background for ulcerative colitis and celiac disease. *Am J Gastroenterol*. 2009;104(7):1737–1744.
7. Wei Y, Lin-Lee YC, Yang X, et al. Molecular cloning of Chinese hamster 1q31 chromosomal fragile site DNA that is important to mdr1 gene amplification reveals a novel gene whose expression is associated with spermatocyte and adipocyte differentiation. *Gene*. 2006;372:44–52.
8. Kuo MT, Wei Y, Yang X, et al. Association of fragile site-associated (FSA) gene expression with epithelial differentiation and tumor development. *Biochem Biophys Res Commun*. 2006;340(3):887–893.
9. Verstreken P, Ohyama T, Haueter C, et al. Tweek, an evolutionarily conserved protein, is required for synaptic vesicle recycling. *Neuron*. 2009;63(2):203–215.
10. Khuong TM, Habets RL, Slabbaert JR, Verstreken P. WASP is activated by phosphatidylinositol-4,5-bisphosphate to restrict synapse growth in a pathway parallel to bone morphogenetic protein signaling. *Proc Natl Acad Sci U S A*. 2010;107(40):17379–17384.
11. Grant BD, Donaldson JG. Pathways and mechanisms of endocytic recycling. *Nat Rev Mol Cell Biol*. 2009;10(9):597–608.
12. Goldenring JR. Recycling endosomes. *Curr Opin Cell Biol*. 2015;35:117–122.

13. Lasser M, Tiber J, Lowery LA. The role of the microtubule cytoskeleton in neurodevelopmental disorders. *Front Cell Neurosci*. 2018;12:165.
14. Romero DM, Bahi-Buisson N, Francis F. Genetics and mechanisms leading to human cortical malformations. *Semin Cell Dev Biol*. 2018;76:33—75.
15. Valente EM, Rosti RO, Gibbs E, Gleeson JG. Primary cilia in neurodevelopmental disorders. *Nat Rev Neurol*. 2014;10(1):27—36.
16. Somers A, Jean JC, Sommer CA, et al. Generation of transgene-free lung disease-specific human induced pluripotent stem cells using a single excisable lentiviral stem cell cassette. *Stem Cell*. 2010;28(10):1728—1740.
17. Schindelin J, Arganda-Carreras I, Frise E, et al. Fiji: an open-source platform for biological-image analysis. *Nat Methods*. 2012;9(7):676—682.
18. Carpenter AE, Jones TR, Lamprecht MR, et al. CellProfiler: image analysis software for identifying and quantifying cell phenotypes. *Genome Biol*. 2006;7(10):R100.
19. Sim NL, Kumar P, Hu J, Henikoff S, Schneider G, Ng PC. SIFT web server: predicting effects of amino acid substitutions on proteins. *Nucleic Acids Res*. 2012;40:W452—W457. Web Server issue.
20. Schwarz JM, Cooper DN, Schuelke M, Seelow D. MutationTaster2: mutation prediction for the deep-sequencing age. *Nat Methods*. 2014;11(4):361—362.
21. Adzhubei IA, Schmidt S, Peshkin L, et al. A method and server for predicting damaging missense mutations. *Nat Methods*. 2010;7(4):248—249.
22. Guichard A, Nizet V, Bier E. RAB11-mediated trafficking in host-pathogen interactions. *Nat Rev Microbiol*. 2014;12(9):624—634.
23. Keeling J, Tsiokas L, Maskey D. Cellular mechanisms of ciliary length control. *Cells*. 2016;5(1).
24. Pedersen LB, Mogensen JB, Christensen ST. Endocytic control of cellular signaling at the primary cilium. *Trends Biochem Sci*. 2016;41(9):784—797.
25. Emmer BT, Maric D, Engman DM. Molecular mechanisms of protein and lipid targeting to ciliary membranes. *J Cell Sci*. 2010;123(Pt 4):529—536.
26. Nagy E, Maquat LE. A rule for termination-codon position within intron-containing genes: when nonsense affects RNA abundance. *Trends Biochem Sci*. 1998;23(6):198—199.
27. Desmet FO, Hamroun D, Lalande M, Collod-Beroud G, Claustres M, Beroud C. Human Splicing Finder: an online bioinformatics tool to predict splicing signals. *Nucleic Acids Res*. 2009;37(9):e67.
28. Liu Z, Chang AN, Grinnell F, et al. Vascular disease-causing mutation, smooth muscle alpha-actin R258C, dominantly suppresses functions of alpha-actin in human patient fibroblasts. *Proc Natl Acad Sci U S A*. 2017;114(28):E5569—E5578.
29. Bunnell TM, Burbach BJ, Shimizu Y, Ervasti JM. beta-Actin specifically controls cell growth, migration, and the G-actin pool. *Mol Biol Cell*. 2011;22(21):4047—4058.
30. Bielas SL, Silhavy JL, Brancati F, et al. Mutations in INPP5E, encoding inositol polyphosphate-5-phosphatase E, link phosphatidyl inositol signaling to the ciliopathies. *Nat Genet*. 2009;41(9):1032—1036.
31. Seaman MN, Gautreau A, Billadeau DD. Retromer-mediated endosomal protein sorting: all WASHed up!. *Trends Cell Biol*. 2013;23(11):522—528.
32. Alekhina O, Burstein E, Billadeau DD. Cellular functions of WASP family proteins at a glance. *J Cell Sci*. 2017;130(14):2235—2241.
33. Burianek LE, Soderling SH. Under lock and key: spatiotemporal regulation of WASP family proteins coordinates separate dynamic cellular processes. *Semin Cell Dev Biol*. 2013;24(4):258—266.
34. Croise P, Estay-Ahumada C, Gasman S, Ory S. Rho GTPases, phosphoinositides, and actin: a tripartite framework for efficient vesicular trafficking. *Small GTPases*. 2014;5, e29469.
35. Posor Y, Eichhorn-Grunig M, Haucke V. Phosphoinositides in endocytosis. *Biochim Biophys Acta*. 2015;1851(6):794—804.
36. Bhattacharyya S, Rainey MA, Arya P, et al. Endocytic recycling protein EHD1 regulates primary cilia morphogenesis and SHH signaling during neural tube development. *Sci Rep*. 2016;6:20727.
37. Clement CA, Ajbro KD, Koefoed K, et al. TGF-beta signaling is associated with endocytosis at the pocket region of the primary cilium. *Cell Rep*. 2013;3(6):1806—1814.
38. Scheidel N, Kennedy J, Blacque OE. Endosome maturation factors Rabenosyn-5/VPS45 and caveolin-1 regulate ciliary membrane and polycystin-2 homeostasis. *EMBO J*. 2018;37(9).
39. Riehle RD, Cornea S, Degterev A. Role of phosphatidylinositol 3,4,5-trisphosphate in cell signaling. *Adv Exp Med Biol*. 2013;991:105—139.
40. Michell RH. Inositol lipids: from an archaeal origin to phosphatidylinositol 3,5-bisphosphate faults in human disease. *FEBS J*. 2013;280(24):6281—6294.
41. Zavodszky E, Seaman MN, Moreau K, et al. Mutation in VPS35 associated with Parkinson's disease impairs WASH complex association and inhibits autophagy. *Nat Commun*. 2014;5:3828.
42. Seaman M, Freeman CL. Analysis of the Retromer complex-WASH complex interaction illuminates new avenues to explore in Parkinson disease. *Commun Integr Biol*. 2014;7, e29483.
43. Freeman C, Seaman MN, Reid E. The hereditary spastic paraplegia protein strumpellin: characterisation in neurons and of the effect of disease mutations on WASH complex assembly and function. *Biochim Biophys Acta*. 2013;1832(1):160—173.
44. Li C, Shah SZ, Zhao D, Yang L. Role of the retromer complex in neurodegenerative diseases. *Front Aging Neurosci*. 2016;8:42.